Quantifying the Importance of Vehicle Ammonia Emissions in an Urban Area of the Northeastern US Utilizing Nitrogen Isotopes

Wendell W. Walters[*1,2], Madeline Karod[1,3], Emma Willcocks[4], Bok H. Baek[5], Danielle E. Blum[2,6], and Meredith G. Hastings[1,2]

[1]Department of Earth, Environmental, and Planetary Sciences, Brown University; Providence, RI 02912, USA.
[2]Institute at Brown for Environment and Society, Brown University; Providence, RI 02912, USA
[3]Chemistry and Physics Department, Simmons University; Boston MA 02215, USA
[4]Program in Biology, Division of Biology and Medicine, Brown University; Providence, RI 02912, USA
[5]Center for Spatial Information, Sciences, and Systems, George Mason University; Fairfax, VA 22030, USA
[6]Department of Chemistry, Brown University; Providence, RI 02916, USA

Correspondence to: Wendell W. Walters (wendell_walters@brown.edu)

Abstract. Atmospheric ammonia (NH_3) is a critical component of our atmosphere that contributes to air quality degradation and reactive nitrogen deposition; however, our knowledge of NH_3 in urban environments remains limited. Year-long ambient NH_3 and related species were measured for concentrations and the nitrogen isotopic compositions ($\delta^{15}N$) of NH_3 and particulate ammonium (pNH_4^+) to understand the temporal sources and chemistry of NH_3 in a northeastern US urban environment. We found that urban NH_3 and pNH_4^+ concentrations were elevated compared to regional rural background monitoring stations, with seasonally significant variations. Local and transported sources of NH_x (NH_3 + pNH_4^+) were identified using polar bivariate and statistical back trajectory analysis, which suggested the importance of vehicles, volatilization, industry, and stationary fuel combustion emissions. Utilizing a uniquely positive $\delta^{15}N(NH_3)$ emission source signature from vehicles, a Bayesian stable isotope mixing model indicates that vehicles contribute 46.8±3.5% (mean±1σ) to the annual background level of urban NH_x, with a strong seasonal pattern with higher relative contribution during winter (56.4±7.6%) compared to summer (34.1±5.5%). The decrease in the relative importance of vehicle emissions during the summer was suggested to be driven by temperature-dependent NH_3 emissions from volatilization sources, seasonal fuel combustion emissions related to energy generation, and change in seasonal transport patterns based on wind direction, back trajectory, and NH_3 emission inventory analysis. This work highlights that reducing vehicle NH_3 emissions should be considered to improve wintertime air quality in this region.

1. Introduction

Ammonia (NH_3) is a critical component of the atmosphere and the global nitrogen cycle (Behera et al., 2013; Galloway et al., 2004). As the primary alkaline atmospheric molecule, NH_3 plays an important role in neutralizing atmospheric acids, leading to fine particulate matter ($PM_{2.5}$), including particulate ammonium (pNH_4^+), which have important implications for air quality, human health, visibility, and climate change (Behera and Sharma, 2010; Updyke et al., 2012; Wang et al., 2015). Agricultural activities, including fertilizer application and livestock waste, dominate the emission of NH_3, accounting for over 60% of the global inventory (Bouwman et al., 1997); however, there are significant NH_3 spatiotemporal variabilities due to its short atmospheric lifetime, typically a few hours to a day, and numerous emission sources (Van Damme et al., 2018). Urban regions have been shown to have elevated levels of NH_3 and nitrogen deposition (Plautz, 2018; Joyce et al., 2020; Hu et al., 2014; Decina et al., 2020, 2017), indicating the potential for important non-agricultural emission sources that may disproportionately impact human and environmental health. In recent years, quantifying surface-level NH_3 and its deposition products in the US has been a focus of several national monitoring networks, including the Ammonia Monitoring Network (AMoN), the Interagency Monitoring of Protected Visual Environments (IMPROVE), the National Atmospheric Deposition Program (NADP), and the Clean Air Status and Trends Network (CASTNET). However, these measurements are typically conducted in rural locations. Long-term records of NH_3 and its deposition products in urban regions are exceedingly scarce, which often leads to models evaluated to observations primarily conducted in rural locations (Paulot et al., 2014).

The NH_3 sources contributing to the urban budget remain contested. Several studies have identified vehicle emissions as a major urban NH_3 emission source (Sun et al., 2017, 2014; Suarez-Bertoa et al., 2014, 2017). In contrast, other studies have suggested that vehicle emissions are relatively unimportant for urban regions and instead have found evidence for significant local and transported emissions due to temperature-dependent volatilization sources (Hu et al., 2014; Yao et al., 2013; Nowak et al., 2006). Recent satellite observations, taking advantage of the COVID-19 lockdown period, have for the first time confirmed vehicle emissions as a significant localized source of NH_3 in an urban region (Cao et al., 2021). However, quantifying the contribution of local urban NH_3 emissions to the urban background is complex as it is coupled to meteorological parameters that influence NH_3 and particulate ammonium (pNH_4^+) partitioning, mixing/dispersion of local emissions, and contributions via long-range transport from agricultural regions (Meng et al., 2011; Walker et al., 2004).

The nitrogen stable isotopic composition ($\delta^{15}N$(‰) = [($^{15}R_{sample}$)/($^{15}R_{reference}$)-1]×1000, where ^{15}R is the ratio of $^{15}N/^{14}N$, and air is the N isotopic reference) may be a useful chemical fingerprinting tool to track source contributions and validate model apportionments of urban NH_3 (Felix et al., 2017, 2013). Indeed, numerous studies have utilized $\delta^{15}N$ of NH_3 and pNH_4^+ for source apportionment (e.g., Felix et al., 2017; Pan et al., 2016; Berner and Felix, 2020; Liu et al., 2018; Pan et al., 2018; Wu et al., 2019; Bhattarai et al., 2020; Xiao et al., 2020; Zhang et al., 2021), taking advantage of the suggested lower $\delta^{15}N$ signatures of agricultural NH_3 emissions relative to fossil fuel combustion (Felix et al., 2013; Chang et al., 2016). In this study, we have characterized the seasonal ambient NH_x (NH_3 + pNH_4^+) source contributions using concentration and isotope measurements at an urban site in Providence, RI, US, using laboratory-verified and field-tested collection techniques shown to quantitatively collect NH_x for accurate and precise $\delta^{15}N$ characterizations (Walters and Hastings, 2018; Walters et al., 2019). The study site is a mid-sized coastal city located within the northeastern US megapolis. This is an important region to monitor because the northeastern US wintertime air quality has not improved as much as expected, despite aggressive reductions of precursor emissions in recent decades (Shah et al., 2018). We have recently characterized the $\delta^{15}N(NH_3)$ from urban vehicle plumes, which has indicated this source to have a unique positive $\delta^{15}N$ signature of 6.6±2.1‰ compared to other NH_3 sources that tend to have negative $\delta^{15}N$ values (Walters et al., 2020). Here we aim to quantify the importance of vehicle NH_3 emissions at our urban site. Our study contributes to the first $\delta^{15}N$ measurements of speciated NH_x in New England and contributes to our understanding of seasonal urban NH_x source apportionment in an environment that particulate nitrate (pNO_3^-) formation is commonly NH_3-limited (Park et al., 2004).

2. Materials, Methods, and Datasets

2.1 Collection of NH_x and Associated Gases and Particles

Simultaneous collections of reactive gases and $PM_{2.5}$ were conducted using a series of coated glass honeycomb denuders and a downstream filter pack housed in a ChemComb Speciation Cartridge. This sampling system has been extensively evaluated for its ability to speciate between inorganic gases and particulate matter for offline concentration determination (Koutrakis et al., 1993, 1988). Additionally, this system is a suitable technique for the characterization of $\delta^{15}N(NH_3)$ and $\delta^{15}N(pNH_4^+)$ with a precision of ±0.8‰ and ±0.9‰ (1σ), respectively (Walters and Hastings, 2018; Walters et al., 2019). Briefly, the sampler consisted of a PTFE-coated inlet to minimize reactive gas loss, a $PM_{2.5}$ impactor plate, a basic-coated honeycomb denuder (2% carbonate (w/v) + 1% glycerol (w/v) in 80:20 water-methanol (v/v) solution) to collect acidic gases including nitric acid (HNO_3) and sulfur dioxide (SO_2), an acid-coated denuder (2% citric acid (w/v) + 1% glycerol (w/v) in 20:80 water-methanol (v/v) solution) to collect NH_3, and a filter pack consisting of a Nylon and 5% (w/v) citric acid-coated cellulose filter for the collection of pNH_4^+. All denuder and filter preparation, handling, and extraction techniques have been previously described (Walters and Hastings, 2018; Walters et al., 2019). The samplers were held vertically to limit the potential for gravitational settling of particles on the denuder surfaces and were housed in a custom-built weather-protected container. Ambient air was sampled at a flow rate of 10 liters per minute. Collections were conducted for 24 h (15:00 to 15:00 the following day) approximately twice per week in Providence, RI, US (41.83 ºN, 71.40 ºW) on the rooftop of a building from February 6, 2018, to February 1, 2019 (Figure 1). The study location is a mid-sized coastal city within New England, with an approximate population of 180,000 and population density of 3,800 per km^2. The monitoring location is in an urban-mixed use region that includes commercial buildings, residential buildings, highways, and industry with some clear NH_3 point sources such as vehicles, residential heating, sewage, and industrial emission.

2.2 Concentration and $\delta^{15}N(NH_x)$ Isotopic Analysis

The concentrations of the denuder and filter extraction solutions were analyzed using colorimetry and ion chromatography analytical techniques. The colorimetric analysis included measurements of [NH_4^+] using the indophenol blue method (i.e., US EPA Method 350.1) and [NO_2^-] via diazotization with sulfanilamide dihydrochloride (i.e., US EPA Method 353.2) that was automated by a discrete UV-Vis spectrophotometer (Westco SmartChem). Anion concentrations that included [Cl^-], [NO_3^-], and [SO_4^{2-}] were analyzed using ion chromatography (Dionex DX500). The limit of detection (LOD) of was approximately 0.5 μmol·L^{-1} for [NH_4^+] and [NO_2^-] and 2 μmol·L^{-1} for [Cl^-], [NO_3^-], and [SO_4^{2-}]. The relative standard deviations for all quantified ions were less than 5%. Laboratory blanks of denuder and filter samples were periodically taken, representing approximately 10% of the collected samples. The blanks were below our LOD, except for [Cl^-] that had a large and variable blank for both the carbonate denuder and Nylon filter, such that this data was not reported in this work.

The determination of $\delta^{15}N$ of the NH_4^+ in the denuder and filter extracts was conducted using a chemical technique that converts NH_4^+ to NO_2^- using an alkaline hypobromite solution and reducing the generated NO_2^- to N_2O using sodium azide in an acetic acid buffer solution (Zhang et al., 2007). The generated N_2O was purified and concentrated using an automated extraction system coupled to a continuous flow Isotope Ratio Mass Spectrometer for $\delta^{15}N$ determination as previously described (Walters and Hastings, 2018). In each sample batch, unknowns were calibrated to two internationally recognized NH_4^+ isotopic reference materials, IAEA-N2 and USGS25, with $\delta^{15}N$ values of 20.3‰ and -30.3‰ (Böhlke et al., 1993; Böhlke and Coplen, 1993), respectively. An in-house NH_4^+ quality control ($\delta^{15}N$ = -1.5‰) and an NO_2^- reference material with a known isotope composition (RSIL-N10219; $\delta^{15}N$= 2.8‰) (Böhlke et al., 2007) were also run intermittently as quality control to monitor the conversion of NO_2^- to N_2O and system stability across runs. Corrections to determine $\delta^{15}N(NH_4^+)$ were performed by accounting for isobaric influences, blank effects, and calibrating the unknowns to the internationally recognized $\delta^{15}N(NH_4^+)$ standards. The correction scheme resulted in an average slope between the measured $\delta^{15}N(N_2O)$ and the standard $\delta^{15}N(NH_4^+)$ values of 0.501 ± 0.024 near the theoretical line of 0.500 for the azide/acetic acid reduction method (Zhang et al., 2007; McIlvin and Altabet, 2005). The pooled standard deviations of the isotopic reference materials were ±0.6‰ (n=62), ±0.7‰ (n=62), ±0.5‰ (n=14), and ±1.3‰ (n=18), for IAEA-N2, USGS25, in-house NH_4^+, and RSIL-N10219, respectively. Due to the numerous steps and potential interferences associated with the employed chemical conversion technique, we established the following quality assurance criteria for our sample unknowns: (1) $[NH_4^+]$ greater than 5 $\mu mol \cdot L^{-1}$ to combat the significant alkaline hypobromite reagent blank, (2) $[NO_2^-]/[NH_4^+]$ ratio less than 5% since NO_2^- is an interferent, and (3) quantitative yield of NH_4^+ to NO_2^- conversion (i.e., incomplete conversion would lead to undesirable $\delta^{15}N$ fractionation). These criteria were met for 90 out of 97 NH_3 samples and 60 out of 97 pNH_4^+ samples. The 7 rejected NH_3 samples were because of criterion 3, while the rejected NH_4^+ samples included 18 from criterion 1, 8 from criterion 2, and 11 from criterion 3. The presence of significant amounts of $[NO_2^-]$ was found exclusively on the Nylon filters, which likely reflect the influence of NO_2 collection as previously demonstrated (Perrino et al., 1988). Replicate measurements of sample unknowns across batch analyses was conducted for approximately 10% of samples and had an average deviation of ±1.4‰.

2.3 Ancillary Datasets

Annual emission data of NH_3 at the county level was accessed from the US EPA National Emission Inventory 2014 (NEI-14), and chemically speciated gridded hourly NH_3 emission data was generated using the Sparse Matrix Operator Kerner Emissions (SMOKE) model (Baek and Seppanen, 2021). The SMOKE processor was initialized using the NEI-2014 emissions modeling platform (EMP) version 7.1, as this was the most recently available NEI at the time of the analysis. The model output was binned by month. Ancillary meteorological parameters were accessed from the Rhode Island Department of Health air monitoring and Chemical Speciation Network (CSN) monitoring station at East Providence (Figure 1). Data were accessed from co-located Ammonia Monitoring Network (AMoN) and Clean Air Status and Trends Network (CASTNET) stations located within New England (US EPA Region 1) for [NH_3] and [pNH_4^+], respectively. These sites included Abington, CT (41.84ºN, 72.01°W), Underhill, VT (44.53ºN, 72.87°W), Woodstock, NH (44.53ºN, 72.87°W), and Ashland, ME (46.60ºN, 68.41°W) (Figure 1). Archived back trajectories and boundary layer heights were computed using the NOAA Air Resource Lab HYSPLIT model (Stein et al., 2015). 72-h back trajectories were calculated arriving at Providence, RI (41.73°N, 71.43°W) using the NAM 12 km meteorology initiated at the end of each sampling period. Atmospheric NH_x has a lifetime typically on the order of 2.1 days (Paulot et al., 2016), such that the chosen trajectory time should account for the potential of long-range transport of NH_x to the sampling site. A new back trajectory was calculated every 3 h for a max of 8 trajectories encompassing the 24 h sampling period at 100 m above ground level.

2.4 Statistical Analyses

Geospatial statistical analysis that included bivariate wind direction and wind speed polar plots and back-trajectory clustering was conducted using the 'open-air' program package using R (Carslaw and Ropkins, 2012). Local NH_x source identification was estimated using the conditional bivariate probability function (CBPF) analysis that provides a conditional probability field for high concentrations dependent on wind speed and direction (Uria-Tellaetxe and Carslaw, 2014). It is defined as the following (Eq. 1):

$$CBPF_{\Delta\theta,\Delta u} = \frac{m_{\Delta\theta,\Delta u | C \geq x}}{n_{\Delta\theta,\Delta u}} \qquad \text{(Eq. 1)}$$

where $m_{\Delta\theta,\Delta u}$ is the number of samples in the wind sector $\Delta\theta$ with wind speed interval Δu having concentration C greater than a threshold value x, $n_{\Delta\theta,\Delta u}$ is the total number of samples in that wind direction-speed interval. The threshold values were set as the top 25% concentration for these analyses. These bivariate polar plots show how a concentration of species varies with wind speed and direction in polar coordinates and are useful in characterizing emission sources (Carslaw and Ropkins, 2012; Carslaw et al., 2006; Tomlin et al., 2009; Zhou et al., 2019). Additionally, source locations that contribute to long-range NH_x transport were evaluated using the potential source contribution function (PSCF). This analysis combines atmospheric concentrations with air mass trajectories and uses residence time information to identify air parcels that contribute to high concentrations at a receptor site (Fleming et al., 2012; Pekney et al., 2006; Begum et al., 2005). The PSCF calculation indicates the probability that a source is located at latitude *i* and longitude *j* and is calculated as the following (Eq. 2):

$$PSCF = \frac{m_{ij}}{n_{ij}} \qquad \text{(Eq. 2)}$$

where n_{ij} is the number of times that the trajectories pass through the cell (i,j) and m_{ij} is the number of times that a source concentration was high when the trajectories passed through the cell (i,j), and the criterion for determining m_{ij} was defined as the 90th percentile (Carslaw and Ropkins, 2012).

3. Results and Discussion

3.1 Urban NH_3 and pNH_4^+ Temporal Concentrations

The urban NH_3 and pNH_4^+ were monitored under a range of meteorological conditions (Figure 2). The annual [NH_3] ranged from 0.234 to 2.94 $\mu g/m^3$ with a mean of 0.890±0.517 $\mu g/m^3$ (n=97), and [pNH_4^+] ranged from 0.019 to 1.62 $\mu g/m^3$ with a mean of 0.412±0.287 $\mu g/m^3$ (n=97). The NH_x partitioning between gas and particle-phase was quantified as fNH_3 (fNH_3 = $[NH_3]_{mol}/([NH_3]_{mol} + [pNH_4^+]_{mol})$ and ranged from 0.307 to 0.972 with an average of 0.688±0.141 (n=97). A strong seasonal pattern was observed for both [NH_3] and fNH_3, with the highest values observed during warmer periods. No significant seasonal pattern was observed for [pNH_4^+] that remained relatively consistent throughout each season and characterized by frequent spike events in cold and warm months, including near July 4th, corresponding to a period of significant firework activity.

The [NH_3] and fNH_3 were positively correlated with temperature (r = 0.66; $p<0.01$ & r = 0.51; $p<0.01$; Figure S1). This relationship was consistent with previous observations in rural and urban locations that suggested [NH_3] to be influenced by temperature-dependent volatilization (e.g., agriculture, vegetation, sewage, and waste) and evaporation from semi-volatile NH_4NO_3 particles (Wang et al., 2015; Hu et al., 2014; Yao et al., 2013; Nowak et al., 2006; Yao and Zhang, 2016). Additionally, [NH_3] was negatively correlated with wind speed (r = -0.42; $p < 0.01$) and mixing height (r = -0.52; $p<0.01$) indicating the importance of dilution and vertical height to near-surface [NH_3]. The measured [pNH_4^+] were not significantly correlated with any meteorological parameter (Figure S1). Instead, the annual and seasonal [pNH_4^+] was closely associated with [pNO_3^-] (r=0.69; $p<0.01$) and [pSO_4^{2-}] (r=0.63; $p<0.01$). This finding is expected due to the role that NH_3 has in neutralizing atmospheric nitric acid and sulfuric acid, leading to pNH_4^+ aerosols in the form of NH_4NO_3, NH_4HSO_4, and NH_4SO_4.

3.2 Comparison of Urban NH_3 and pNH_4^+ to Regional Observations

The measured urban [NH_3] and [pNH_4^+] data from Providence, RI, US were compared with the nearby regional observations from AMoN/CASTNET sites within New England (Figure 1 & Figure 3). Overall, the annual average [NH_3] in Providence, RI, was significantly greater ($p<0.05$) than the regional New England AMoN sites. This finding was generally consistent with the NEI-14 estimates for New England, which tends to show that annual NH_3 emission densities were highest for regions near urban locations (Figure 1). [NH_3] grouped by season indicates subtle differences in the seasonal profiles at the varying New England sites (Figure 3A). [NH_3] at Providence, RI was statistically higher ($p<0.05$) during winter and autumn than the New England AMoN sites and higher than all sites except for Abington, CT, during summer. During spring, [NH_3] at Providence, RI, was not statistically different from any of the New England AMoN sites, which typically exhibited a springtime [NH_3] peak that likely reflects the influence and timing of fertilizer application (Felix et al., 2017). We note that there can be large heterogeneity in urban [NH_3]; however, the Providence, RI monitoring site was specifically chosen since it was away from any direct emission sources and at a raised elevation. The difference in our measured [NH_3] and reported by AMoN are unlikely to be explained by differences in sampling methodology. We have recently demonstrated that our active denuder sampling technique resulted in NH_3 concentrations within 2-5% of that determined from simultaneous deployed passive NH_3 collection techniques, which are utilized at AMoN sites (Walters et al., 2020). This result was consistent with previous comparisons between active and passive NH_3 sampling techniques (Zhou et al., 2019; Puchalski et al., 2015).

The annual average [pNH_4^+] at the Providence, RI site was also found to be significantly higher than the regional CASTNET sites ($p<0.05$; Fig. 3B). However, when broken down by season, the Providence, RI site has significantly higher [pNH_4^+] than all the regional CASTNET sites only during autumn ($p <0.05$). During the winter and summer, the Providence, RI site did not have significantly higher [pNH_4^+] than any of the CASTNET sites. During the spring, [pNH_4^+] was higher in Providence, RI, than the two most remote regional CASTNET sites, including Ashland, ME, and Woodstock, NH ($p<0.05$), but not significantly different from the Abington, CT or Underhill, VT sites. It is important to note that methodology differences in the collection of pNH_4^+ could have significantly influenced the [pNH_4^+] annual differences and seasonal patterns. Our collection method (Nylon filter + acid-coated filter) should lead to the quantitative collection of pNH_4^+ (Walters et al., 2019; Yu et al., 2006). In contrast, pNH_4^+ collections at the CASTNET sites utilize PTFE filters which could be biased low due to the potential for significant loss of semi-volatile NH_4NO_3 (Ashbaugh and Eldred, 2004; Yu et al., 2005). The potential for NH_4NO_3 volatilization should be more significant for warmer temperatures (Ashbaugh and Eldred, 2004; Yu et al., 2005). However, we did not observe a significant difference in summer [pNH_4^+] between the Providence, RI, and regional CASTNET sites. Thus, the influence of sampling methodologies on the spatiotemporal [pNH_4^+] patterns remains difficult to quantify.

Localized NH_3 emissions likely play an important role in contributing to the observed elevated urban [NH_x] and the spatiotemporal patterns across New England (Figure 4). The NEI-14 emission profiles at the AMoN sites indicated that agricultural activities drive the seasonal NH_3 emissions, while non-agricultural sources, including stationary fuel combustion (electricity generating units and residential heating) and vehicles, were important during winter but their relative contributions significantly decreased during warmer periods. In contrast, the annual NH_3 emission in Providence, RI were dominated by fuel combustion emissions. The total NH_3 emission density in Providence, RI had less seasonal variability than the regional AMoN/CASTNET locations despite a potential seasonal change in emissions with relatively high contributions from residential heating (i.e., oil, gas, wood combustion) during winter compared with summer. We note that natural gas and oil stationary fuel combustion, which is predicted to be the main NH_3 emission source at our urban study site as well as in other major urban areas in regions with a large heating demand (Zhou et al., 2019), has a highly uncertain NH_3 emission factor established from limited studies conducted before 1982 (Muzio and Arand, 1976; Cass et al., 1982). Additionally, it has been recently pointed out that vehicle NH_3 emission, another major source of urban NH_3, might be underpredicted by at least a factor of 2 in the NEI (Sun et al., 2017; Fenn et al., 2018).

3.3 Urban $\delta^{15}N$ of Urban NH_x

Measurements of $\delta^{15}N$ at the Providence, RI monitoring site were utilized to enhance understanding of source contributions to urban NH_x. The measured $\delta^{15}N(NH_3)$ ranged from -21.4 to -2.0‰ with an average of -11.9±5.0‰ (n=90), and $\delta^{15}N(pNH_4^+)$ ranged from -7.4 to 17.5‰ with a mean of 4.9±6.2‰ (n=60) (Figure 5). The measured $\delta^{15}N$ data was binned by season that included winter (Dec, Jan, Feb), spring (Mar, Apr, May), summer (Jun, Jul, Aug), and autumn (Sep, Oct, Nov). The $\delta^{15}N(NH_3)$ was statistically higher during spring (-7.6±3.5‰, n=21 ($\bar{x}\pm1\sigma$)) compared to the other seasons (summer = -13.9±4.1‰, n=21; autumn = -13.1±5.1‰, n=21; winter = -13.4±5.2‰, n=18, $p<0.05$). The $\delta^{15}N(pNH_4^+)$ also indicated significant seasonality with lower values during summer (0.4±4.9‰, n=18) compared to autumn (7.4±4.8‰, n=15) and winter (9.0±5.8‰; n=14) ($p<0.05$). However, springtime $\delta^{15}N(pNH_4^+)$ (4.1±5.2‰, n=13) was not statistically different from any season.

The $\delta^{15}N$ of atmospheric NH_3 and pNH_4^+ reflects a combination of source effects from different NH_3 emission sources and isotopic equilibrium between NH_3 and pNH_4^+ that has been shown to have a large influence on setting the N isotopic distribution between these molecules (Walters et al., 2018; Savard et al., 2017; Kawashima and Ono, 2019). Indeed, the annual $\delta^{15}N(pNH_4^+)$ was statistically higher than $\delta^{15}N(NH_3)$ ($p<0.01$), reflecting the contributions from the nitrogen isotope exchange reactions between NH_3 and NH_4^+, which tends to elevate the $\delta^{15}N(pNH_4^+)$ relative to $\delta^{15}N(NH_3)$ (Walters et al., 2018; Kawashima and Ono, 2019; Urey, 1947). The isotope difference or isotope enrichment factor ($^{15}\varepsilon_{pNH4+/NH3}$) between $\delta^{15}N(pNH_4^+)$ and $\delta^{15}N(NH_3)$ was calculated as the following (Eq. 3):

$$\Delta\delta^{15}N \approx {}^{15}\varepsilon_{pNH_4^+/NH_3} = \delta^{15}N(pNH_4^+) - \delta^{15}N(NH_3) \qquad \text{(Eq. 3)}$$

The $\Delta\delta^{15}N$ ranged from -0.1 to 34.1‰ and averaged 17.6±7.8‰ (n=56) (Figure 6). There was a strong seasonal $\Delta\delta^{15}N$ pattern with higher values during colder periods, and $\Delta\delta^{15}N$ was weakly correlated with temperature (r = -0.55, p <0.01; Fig. S1), suggesting that these values were difficult to predict. The observed $\Delta\delta^{15}N$ was significantly lower than the expected temperature-dependent theoretical isotopic equilibrium values between NH_3 and NH_4^+ of 35±3‰ at 25 ºC (Walters et al., 2018) and previous field $\Delta\delta^{15}N$ observations (Savard et al., 2017), indicating that incomplete isotopic equilibrium between NH_3 and pNH_4^+ was achieved at the study site. This result has important implications for previous $\delta^{15}N$ source apportionment studies of NH_3 and pNH_4^+, which commonly utilize an assumed and theoretically calculated phase-dependent fractionation (e.g., Zhang et al., 2021; Pan et al., 2016; Gu et al., 2022a, b; Berner and Felix, 2020). A potential explanation for the observed incomplete isotopic equilibrium would be that localized NH_3 emissions perturbed the isotopic equilibrium between NH_3 and $pNH_4^{+,}$ which may take tens of minutes to several hours to be achieved (Kim et al., 1993). Indeed, previously laboratory dynamic flow chamber experiments have demonstrated that fresh NH_3 emissions tend to result in $\Delta\delta^{15}N$ values below the theoretically predicted value (Kawashima and Ono, 2019). Additionally, there may be other contributing isotope effects between NH_3 and pNH_4^+ such as the hypothesized kinetic isotope effect associated with NH_3 diffusion to an aerosol surface leading to a lower $\delta^{15}N(pNH_4^+)$ value compared to $\delta^{15}N(NH_3)$ (Pan et al., 2016). The observed $\Delta\delta^{15}N$ seasonality remains difficult to explain. Still, we speculate that it may be related to higher localized emissions of NH_3 during warmer periods that perturb the NH_3/pNH_4^+ isotope equilibrium and/or seasonal changes in PM chemical compositions (Pan et al., 2016), such as higher NH_4NO_3 during colder months.

To account for the complex phase-dependence on $\delta^{15}N$ variabilities, we calculated $\delta^{15}N(NH_x)$ according to the following (Eq. 4):

$$\delta^{15}N(NH_x) = fNH_3 \times \delta^{15}N(NH_3) + (1 - fNH_3) \times \delta^{15}N(NH_4^+) \qquad \text{(Eq. 4)}$$

The annual $\delta^{15}N(NH_x)$ ranged from -17.4 to 6.3‰ and averaged -6.0±4.9‰ (n=56) (Figure 5). There was significant seasonality with lower values during summer (-9.0±4.2‰, n=18) compared to winter (-3.4±5.3‰, n=13) and spring (-3.8±3.3‰, n=10). The autumn $\delta^{15}N(NH_x)$ (-6.2±4.1‰, n=15) was not significantly different from any season. The $\delta^{15}N(NH_x)$ is independent of the phase $\delta^{15}N$ fractionation, such that it should be a robust tracer reflecting the integrated source contributions and physical processing from locally emitted and transported NH_3 and pNH_4^+. Therefore, the $\delta^{15}N(NH_x)$ observations would suggest a seasonal change in sources of NH_x with increased relative emissions from a source with a high $\delta^{15}N(NH_3)$ value during the colder periods of winter and spring and a lower $\delta^{15}N(NH_3)$ value during summer. Vehicle emissions have an elevated $\delta^{15}N(NH_3)$ value of 6.6±2.1‰ (Walters et al., 2020; Song et al., 2021), such that the relative importance of vehicle emissions to NH_x in Providence, RI may have increased during colder seasons. The observed $\delta^{15}N(NH_x)$ decrease during summer and increase in $[NH_3]$ might suggest increased emissions from temperature-dependent emission sources with a relatively low $\delta^{15}N(NH_3)$ signature, such as volatilization (Felix et al., 2013; Freyer, 1978; Heaton, 1987; Chang et al., 2016; Hristov et al., 2009). There were often large $\delta^{15}N(NH_x)$ variations within each season, which may be related to wind direction shifts and varying contributions from local urban NH_3 emission sources and long-range transport of NH_x.

The physical processing of NH_3 could have also played an important role in the observed $\delta^{15}N(NH_x)$ seasonal trends. The enrichment factor associated with NH_3 dry deposition has not been measured directly. Still, it has been suggested to be low (~ 4‰) based on the physical processing of NH_3 in a vehicle tunnel (Walters et al., 2020). This result would suggest that as NH_3 undergoes dry deposition, the pool of $\delta^{15}N(NH_3)$ in the atmosphere becomes slightly depleted as the heavier $^{15}NH_3$ is preferentially deposited. The increased temperatures during summer and autumn would have increased the amount of dry deposited NH_3 that re-volatilized into the atmosphere (Behera et al., 2013). NH_3 volatilization has been shown to have a significant fractionation effect leading to the emission of NH_3 depleted in ^{15}N (Hristov et al., 2009; Frank et al., 2004). Further work is needed to refine our understanding of NH_3 bidirectional exchange and its impact on $\delta^{15}N$; however, we expect this process would have contributed to lower $\delta^{15}N(NH_x)$ values during the warmer periods due to increased temperature-dependent NH_3 volatilization.

3.4 Identifying Urban Local Sources of NH_x

Wind data and bivariate plot statistical analysis were utilized to investigate local and transported sources of urban NH_x. The local wind data indicated a clear shift in wind direction and speed from generally faster winds from the west/northwest during winter to slower winds from the south/southeast and northeast during summer (Figure 7). Wind direction and wind speed polar bivariate CBPF plots of [NH_3] and [pNH_4^+] indicated relative high probability under conditions of low wind speeds (i.e., < 2 m/s) for all seasons, suggesting the importance of local emitted NH_3 sources and pNH_4^+ formation. These elevated CBPF probabilities were also associated with winds from the southeast to west, the direction of I-195 and I-95, major interstate highways, and industrial sources (Figure 1). The highest $\delta^{15}N(NH_x)$ values within each season were observed with winds from these directions, implicating the importance of vehicle emissions, which have an elevated $\delta^{15}N(NH_3)$ signature of 6.6±2.1‰ compared to other NH_3 sources that tend to have $\delta^{15}N(NH_3)$ values below 0‰, including available industrial $\delta^{15}N(NH_3)$ emissions (Walters et al., 2020).

Additionally, high CPF probabilities for both [NH_3] and [pNH_4^+] were observed during the warmer seasons of summer and autumn from moderate winds (2-4 m/s) from the northeast and west. This result may implicate local temperature-dependent NH_3 emission sources such as sewage lines, trash cans, soil emissions from green spaces, and regional transport (Hu et al., 2014; Sutton et al., 2000; Pandolfi et al., 2012; Reche et al., 2012; Meng et al., 2011; Galán Madruga et al., 2018; Zhou et al., 2019). These winds were associated with a relatively low $\delta^{15}N(NH_x)$, consistent with volatilization contributions with a low $\delta^{15}N(NH_3)$ emission signature between -56.1 to -10.3‰ based on livestock waste and fertilizer studies (Heaton, 1987; Freyer, 1978; Felix et al., 2013; Chang et al., 2016). Low CPF probabilities for both [NH_3] and [pNH_4^+] were generally associated with high wind speeds (i.e., > 4 m/s), reflecting the dilution of these pollutants and strong background mixing. An exception to this trend was observed for [pNH_4^+] during the winter, with elevated CPF probabilities with high wind speeds indicating the importance of long-range transport. Interestingly, there was a seasonal difference in $\delta^{15}N(NH_x)$ from this wind profile, with high values during the cold seasons and low values during summer, suggesting that the background NH_x had larger contributions from vehicle emissions and volatilization during the cold and warm seasons, respectively.

3.5 Role of Long-Range Transport as a Source of Urban NH_x

Air mass back trajectories and PSCF analysis were utilized to identify source locations of transported NH_3 and pNH_4^+ to Providence, RI. The clustered seasonal air mass back trajectories indicated a shift in the seasonal air mass origin, with winds originating from the north and west during winter with higher contributions of air masses derived from the south and along the coast during summer (Figure 8). During summer and autumn, potentially significant NH_3 and pNH_4^+ source regions originated over the mid-Atlantic, midwestern US, Atlantic coast, southeastern US, southeastern Ontario, and southeastern Quebec. These regions have significant agricultural-related NH_3 emissions, such as fertilizer application, livestock waste, and significant urban and industrial activities. Transport from these regions tended to have relatively low mean $\delta^{15}N(NH_x)$ values (i.e., -15 to -5‰), consistent with transport of volatilized agricultural NH_3 emissions that favor the release of isotopically light $^{14}NH_3$ (Heaton, 1987; Freyer, 1978; Felix et al., 2013; Chang et al., 2016) and available industrial emissions with a reported low $\delta^{15}N(NH_3)$ values of -20.1‰ from a steel factory (Heaton, 1987). We also note that NH_3 deposition and re-volatilization during transport of any NH_3 emission source may also lead to significant isotope fractionation as NH_3 is transported downwind. Because NH_3 volatilization has been shown to lead to the initial release of NH_3 depleted in ^{15}N, it is reasonable to assume that this long-range transported NH_3 would contribute low $\delta^{15}N(NH_3)$ (Frank et al., 2004; Hristov et al., 2009). Thus, low $\delta^{15}N(NH_3)$ values from the identified important contribution regions during the warmer seasons may also reflect the bidirectional exchange of NH_3 as it is long-range transported downwind from agricultural, urbanized, and industrialized regions. Available ground-based monitoring data indicates the identified source regions tend to have elevated ambient [NH_3] and [pNH_4^+], consistent with these regions as potential NH_3 and pNH_4^+ source contributors to Providence, RI (Figure S2). Additionally, the Atlantic coast may represent contributions from ocean NH_3 flux expected to increase during warmer periods (Paulot et al., 2015), which has been suggested to have low $\delta^{15}N$ values (Jickells et al., 2003).

Elevated PSCF probabilities were identified for [pNH_4^+] during the winter from the mid-Atlantic and Midwestern US, which is consistent with available [pNH_4^+] ground-based observations that tend to peak during this period due to ambient conditions that favor the formation of NH_4NO_3 (Figure S2). This transport region tended to have relatively high mean $\delta^{15}N(NH_x)$ values (e.g., -5 to 0‰) from the Midwestern US and relatively low mean from the Mid-Atlantic (~-10‰). Across the US, [NH_3] was lowest during winter due to decreased agricultural activities (Figure S2). Indeed, the NEI-14 indicates that the relative importance of non-agricultural NH_3 sources increases during winter (Figure 4), such that the higher $\delta^{15}N(NH_x)$ values deriving from the Midwest may reflect the regional importance of sources with an elevated $\delta^{15}N(NH_3)$ value such as vehicles and/or fuel-combustion. Lower mean $\delta^{15}N(NH_x)$ values derived from the mid-Atlantic may suggest that agricultural emissions such as animal housing remain an important wintertime NH_x source contributor to Providence, RI. Additionally, there could be contributions from stationary fuel combustion that have a reported $\delta^{15}N(NH_3)$ signature of -14.6 to -11.3‰ (Felix et al., 2013), and contributions from upwind volatilized NH_3 emissions from Canada.

3.6 Urban NH_x Source Apportionment

The NH_x source contributions at Providence, RI, including local and transported emissions, were quantified using SIMMR (Parnell et al., 2010). The model was initiated using the measured $\delta^{15}N(NH_x)$ values and assuming vehicles, volatilization, stationary fuel combustion (i.e., residential fuel combustion, industrial fuel combustion, energy generating units), and industry were the main sources, as evidenced by the local wind direction and back trajectory analysis and the NEI-14 predictions. We acknowledge that there are additional miscellaneous NH_3 sources in an urban environment, including pets, household products, humans, and wood combustion (Ampollini et al., 2019; Sutton et al., 2000; Li et al., 2020); however, we assumed that these sources were negligible compared to the main identified emission sources.

The source apportionment results are sensitive to the number of considered sources, their designated $\delta^{15}N(NH_3)$ emission signatures, and uncertainty. The input $\delta^{15}N(NH_3)$ emission source signatures were deliberately chosen from sampling methodologies that have utilized active sampling approaches, as it has been well-documented from several studies that passive samplers result in a $\delta^{15}N(NH_3)$ bias and could be unreliable (Pan et al., 2020; Kawashima et al., 2021; Walters et al., 2020). Fertilization application is a significant source of NH_3 emissions globally and within the US. However, fertilizer application represents a small component of the overall agricultural emissions at our site (~1.8%) and within our region (7.1%; US EPA Region 1) based on the NEI-14. Further, fertilization-related NH_3 emissions tend to peak during spring; however, we neither identified any significant NH_x long-range transport region nor observed a relative decrease in $\delta^{15}N(NH_x)$ during spring, which would be consistent with a suspected low fertilizer volatilization $\delta^{15}N(NH_3)$ emission signature. Thus, fertilizer application was not directly considered in our source apportionment model but lumped into the considered volatilization category.

The input source values for vehicles, stationary fuel combustion/industry, and volatilization were fixed at 6.6±2.1‰ (Walters et al., 2020), -15.3±3.6‰ (Heaton, 1987; Freyer, 1978), and -19.2±8.3‰ (Freyer, 1978; Heaton, 1987; Hristov et al., 2009; Frank et al., 2004). Stationary fuel combustion and industry $\delta^{15}N(NH_3)$ emission signatures were grouped due to their similar values (Text S1). The volatilization $\delta^{15}N(NH_3)$ emission signature represents integrated volatilization measurements conducted in animal sheds (Freyer, 1978; Heaton, 1987), and measurements that include monitoring volatilization as a function of time, which indicate significant $\delta^{15}N(NH_3)$ variability (Hristov et al., 2009; Frank et al., 2004). The volatilization category represented waste volatilization from agricultural activities and urban sources (i.e., sewer, trash, green spaces) and transported NH_3 that has re-volatilized to the atmosphere because of NH_3 bidirectional exchange. Further details on our rationale for the chosen source $\delta^{15}N$ values are provided in the Supporting Information (Text S1).

The mixing model predicts the relative fractional contributions of vehicles, volatilization, and stationary fuel combustion/industry emissions of (mean±σ) 46.8±3.5%, 26.3±12.3%, and 26.9±14.4% to the annual NH_x background in Providence, RI (Figure 9A). The relative contribution of vehicle emissions had a strong seasonal profile with higher contributions during the colder seasons of winter (56.4±7.6%) and spring (55.4±5.8%) compared to the warmer seasons of summer (34.1±5.5%) and autumn (45.4±5.5%). The relative contribution for volatilization and stationary fuel combustion/industry was predicted to peak during summer with means of 31.7±15.4% and 34.2±18.2%, compared to winter with means of 20.9±10.3%, 22.6±12.1%, respectively. The annual and seasonal mass-weighted contributions of the considered sources were calculated utilizing the NH_x concentrations (Figure 9B). Overall, vehicles tended to be a consistent source of urban NH_x with contributions of 35.2±2.6, 33.3±3.5, 32.8±5.3, 35.2±4.3, and 35.4±4.8 nmol/m^3 for the annual, spring, summer, autumn, and winter, respectively. The mass-weighted contributions for both volatilization and fuel combustion follow their relative fractional profiles with significant seasonal patterns that peaked during summer compared to winter, respectively. Based on the NEI-14, wind direction, and long-range transport analysis (Figures 4, 7, & 8), we suspect the relative contribution of vehicle emissions diminished during summer due to the increased importance of temperature-dependent NH_3 volatilization emissions, increased energy consumption due to cooling demands, and/or change in transport over heavily industrialized regions such as heavily urbanized Toronto and the East Coast shoreline. The exact NH_3 volatilization source remains unclear. However, there was evidence of significant contributions from local urban volatilization (i.e., sewage, waste, urban green spaces) and long-range transport from regional agricultural regions and over the ocean.

The source apportionment results were compared with the predicted NH_3 emissions from the NEI-14. We acknowledge that this comparison may not yield quantitative results because the NEI-14 was at a country-level resolution, and our single study site may not represent all the county-level NH_3 emission predictions; however, this comparison may yield a qualitative understanding in the uncertainties of urban NH_x. Overall, the seasonally consistent mass-weighted contribution of vehicle emissions from the mixing model source apportionment results was consistent with the NEI-14 that predicts nearly uniform vehicle emissions throughout the year (Figure 4). However, the NEI-14 predicts a much slightly lower contribution of annual vehicle emissions in our study location of 31.9% compared to our mixing model results (46.8±3.5%). Our mixing model source apportionment results indicate a relatively low fractional and mass-weighted contribution for stationary fuel combustion for winter. In contrast the NEI-14 indicated that residential fuel (natural gas and oil) combustion was the largest emission source of NH_3 at our study site, the rural CASTNET sites, and other cities during periods of significant heating demands (Zhou et al., 2019). While we acknowledge that the stationary fuel combustion $\delta^{15}N(NH_3)$ emission signatures were uncertain, the mixing model and seasonal [NH_3] results would suggest that residential NH_3 emissions were overpredicted in the NEI-14, while vehicle emissions may be underpredicted. Thus, vehicle and fuel combustion emission factors may need to be revisited to more accurately model urban [NH_3] and predict its human and ecological impacts.

4. Conclusion

Elevated urban NH_x concentrations were observed in Providence, RI, relative to regional background monitoring stations in New England. Mixing model $\delta^{15}N(NH_x)$ source apportionment results utilizing $\delta^{15}N(NH_x)$, suggest that vehicles represent an important source of urban NH_x with strong seasonal variability. The relative contribution of vehicle emissions was highest during winter/spring, which is significant because NH_3 emissions may contribute to the elevated $PM_{2.5}$ observed during this time in the eastern US (Shah et al., 2018). Reductions in vehicle ammonia emissions may represent a promising way to mitigate the adverse impacts of elevated urban NH_3 concentrations and yield positive benefits for ecosystems and human health. However, vehicle NH_3 emissions result from the technology used to combat vehicle NO_x and CO emissions. Decreasing vehicle NH_3 emissions may not be achievable until vehicle fleet electrification. Expanding national observational networks to include urban measurements of [NH_3] and $\delta^{15}N(NH_x)$ are needed to monitor urban trends and design future regulatory NH_3 fossil-fuel-related emission reductions.

This work demonstrated that nitrogen isotopic analysis allows for further refinement of our understanding and quantification of urban NH_x sources, laying the foundation for future source apportionment studies. Utilizing a laboratory-verified collection method suitable for NH_x speciation and isotope analysis was critical for accurate source apportionment due to the observed complex phase-dependent $\delta^{15}N$ isotope fractionation between NH_3 and pNH_4^+. Future studies should improve our understanding of the drivers behind NH_3 and pNH_4^+ phase $\delta^{15}N$ fractionation, including controlled chamber studies and field observations, which may also provide important insights into controls on NH_3/pNH_4^+ gas to particle-phase conversion. Still, this work highlights the need to improve our $\delta^{15}N(NH_3)$ emission source values, particularly for our volatilization, industry, and fuel combustion sources, to enhance the quality of the source apportionment results.

Data Availability. Data presented in this article are available on the Harvard Dataeverse at https://doi.org/10.7910/DVN/JHMBRI and in the Supplement .

Author contributions. WWW, MK, and MGH designed varying aspects of the field sampling plan. WWW, MK, and DEB carried out the field measurements. WWW, MK, and DEB conducted all laboratory analyses of data. EW contributed spatial analysis of data. BHB contributed emission modeling of the presented data. WWW prepared the article with contributions from all co-authors.

Competing interests. The authors declare that they have no conflict of interest.

Acknowledgements. We thank Ruby Ho for sampling and laboratory assistance. We are grateful to Paul Theroux of RI-DEM/RI-DOH for access and support at the RI-DEM air-monitoring sites.

Financial support. This research has been supported by the National Science Foundation Division of Atmospheric and Geospace Sciences (grant: 1624618) and the Institute at Brown for Environment and Society (internal grant no. GR300123).

References

Ampollini, L., Katz, E. F., Bourne, S., Tian, Y., Novoselac, A., Goldstein, A. H., Lucic, G., Waring, M. S., and DeCarlo, P. F.: Observations and Contributions of Real-Time Indoor Ammonia Concentrations during HOMEChem, Environ. Sci. Technol., 53, 8591–8598, 2019.

Ashbaugh, L. L. and Eldred, R. A.: Loss of particle nitrate from teflon sampling filters: effects on measured gravimetric mass in California and in the IMPROVE network, J Air Waste Manag Assoc, 54, 93–104, 2004.

Baek, B. H. and Seppanen, C.: CEMPD/SMOKE: SMOKE v4.8.1 Public Release (January 29, 2021), 2021.

Begum, B. A., Kim, E., Jeong, C.-H., Lee, D.-W., and Hopke, P. K.: Evaluation of the potential source contribution function using the 2002 Quebec forest fire episode, Atmospheric Environment, 39, 3719–3724, 2005.

Behera, S. N. and Sharma, M.: Investigating the potential role of ammonia in ion chemistry of fine particulate matter formation for an urban environment, Science of the Total Environment, 408, 3569–3575, 2010.

Behera, S. N., Sharma, M., Aneja, V. P., and Balasubramanian, R.: Ammonia in the atmosphere: a review on emission sources, atmospheric chemistry and deposition on terrestrial bodies, Environmental Science and Pollution Research, 20, 8092–8131, 2013.

Berner, A. H. and David Felix, J.: Investigating ammonia emissions in a coastal urban airshed using stable isotope techniques, Science of The Total Environment, 707, 134952, 2020.

Bhattarai, N., Wang, S., Xu, Q., Dong, Z., Chang, X., Jiang, Y., and Zheng, H.: Sources of gaseous NH_3 in urban Beijing from parallel sampling of NH_3 and NH_4^+, their nitrogen isotope measurement and modeling, Science of the Total Environment, 747, 141361, 2020.

Böhlke, J. K. and Coplen, T. B.: Reference and intercomparison materials for stable isotopes of light elements, in: Proceedings of the IAEA-TECDOC-825 Consultants Meeting Held in Vienna, Vienna, Austria, 1993.

Bohlke, J. k., Gwinn, C. j., and Coplen, T. b.: New Reference Materials for Nitrogen-Isotope-Ratio Measurements, Geostandards Newsletter, 17, 159–164, 1993.

Böhlke, J. K., Smith, R. L., and Hannon, J. E.: Isotopic analysis of N and O in nitrite and nitrate by sequential selective bacterial reduction to N_2O, Analytical chemistry, 79, 5888–5895, 2007.

Bouwman, A. F., Lee, D. S., Asman, W. A. H., Dentener, F. J., Van Der Hoek, K. W., and Olivier, J. G. J.: A global high-resolution emission inventory for ammonia, Global biogeochemical cycles, 11, 561–587, 1997.

Cao, H., Henze, D. K., Cady-Pereira, K., McDonald, B. C., Harkins, C., Sun, K., Bowman, K. W., Fu, T.-M., and Nawaz, M. O.: COVID-19 Lockdowns Afford the First Satellite-Based Confirmation That Vehicles Are an Under-recognized Source of Urban NH_3 Pollution in Los Angeles, Environmental Science & Technology Letters, 2021.

Carslaw, D. C. and Ropkins, K.: Openair—an R package for air quality data analysis, Environmental Modelling & Software, 27, 52–61, 2012.

Carslaw, D. C., Beevers, S. D., Ropkins, K., and Bell, M. C.: Detecting and quantifying aircraft and other on-airport contributions to ambient nitrogen oxides in the vicinity of a large international airport, Atmospheric Environment, 40, 5424–5434, 2006.

Cass, G. R., Gharib, S., Peterson, M., and Tilden, J. W.: The origin of ammonia emissions to the atmosphere in an urban area, Open file report, 82–6, 1982.

Chang, Y., Liu, X., Deng, C., Dore, A. J., and Zhuang, G.: Source apportionment of atmospheric ammonia before, during, and after the 2014 APEC summit in Beijing using stable nitrogen isotope signatures, Atmospheric Chemistry and Physics, 16, 11635–11647, 2016.

Decina, S. M., Templer, P. H., Hutyra, L. R., Gately, C. K., and Rao, P.: Variability, drivers, and effects of atmospheric nitrogen inputs across an urban area: emerging patterns among human activities, the atmosphere, and soils, Science of the Total Environment, 609, 1524–1534, 2017.

Decina, S. M., Hutyra, L. R., and Templer, P. H.: Hotspots of nitrogen deposition in the world's urban areas: a global data synthesis, Frontiers in Ecology and the Environment, 18, 92–100, 2020.

Felix, D. J., Elliott, E. M., Gish, T. J., McConnell, L. L., and Shaw, S. L.: Characterizing the isotopic composition of atmospheric ammonia emission sources using passive samplers and a combined oxidation-bacterial denitrifier approach, Rapid Communications in Mass Spectrometry, 27, 2239–2246, 2013.

Felix, J. D., Elliott, E. M., and Gay, D. A.: Spatial and temporal patterns of nitrogen isotopic composition of ammonia at U.S. ammonia monitoring network sites, Atmospheric Environment, 150, 434–442, 2017.

Fenn, M. E., Bytnerowicz, A., Schilling, S. L., Vallano, D. M., Zavaleta, E. S., Weiss, S. B., Morozumi, C., Geiser, L. H., and Hanks, K.: On-road emissions of ammonia: An underappreciated source of atmospheric nitrogen deposition, Science of The Total Environment, 625, 909–919, 2018.

Fleming, Z. L., Monks, P. S., and Manning, A. J.: Untangling the influence of air-mass history in interpreting observed atmospheric composition, Atmospheric Research, 104, 1–39, 2012.

Frank, D. A., Evans, R. D., and Tracy, B. F.: The role of ammonia volatilization in controlling the natural 15N abundance of a grazed grassland, Biogeochemistry, 68, 169–178, 2004.

Freyer, H. D.: Seasonal trends of NH_4^+ and NO_3^- nitrogen isotope composition in rain collected at Jülich, Germany, Tellus, 30, 83–92, 1978.

Galán Madruga, D., Fernandez Patier, R., Puertas, S., García, R., and Cristóbal López, A.: Characterization and local emission sources for ammonia in an urban environment, Bulletin of environmental contamination and toxicology, 100, 593–599, 2018.

Galloway, J. N., Dentener, F. J., Capone, D. G., Boyer, E. W., Howarth, R. W., Seitzinger, S. P., Asner, G. P., Cleveland, C., Green, P., and Holland, E.: Nitrogen cycles: past, present, and future, Biogeochemistry, 70, 153–226, 2004.

Gu, M., Pan, Y., Sun, Q., Walters, W. W., Song, L., and Fang, Y.: Is fertilization the dominant source of ammonia in the urban atmosphere?, Science of The Total Environment, 838, 155890, 2022a.

Gu, M., Pan, Y., Walters, W. W., Sun, Q., Song, L., Wang, Y., Xue, Y., and Fang, Y.: Vehicular Emissions Enhanced Ammonia Concentrations in Winter Mornings: Insights from Diurnal Nitrogen Isotopic Signatures, Environ. Sci. Technol., 56, 1578–1585, 2022b.

Heaton, T. H. E.: $^{15}N/^{14}N$ ratios of nitrate and ammonium in rain at Pretoria, South Africa, Atmospheric Environment (1967), 21, 843–852, 1987.

Hristov, A. N., Zaman, S., Vander Pol, M., Ndegwa, P., Campbell, L., and Silva, S.: Nitrogen losses from dairy manure estimated through nitrogen mass balance and chemical markers, Journal of environmental quality, 38, 2438–2448, 2009.

Hu, Q., Zhang, L., Evans, G. J., and Yao, X.: Variability of atmospheric ammonia related to potential emission sources in downtown Toronto, Canada, Atmospheric Environment, 99, 365–373, 2014.

Jickells, T. D., Kelly, S. D., Baker, A. R., Biswas, K., Dennis, P. F., Spokes, L. J., Witt, M., and Yeatman, S. G.: Isotopic evidence for a marine ammonia source, Geophys. Res. Lett., 30, 1374, 2003.

Joyce, E. E., Walters, W. W., Roy, E. L., Clark, S. C., Schiebel, H., and Hastings, M. G.: Highly concentrated atmospheric inorganic nitrogen deposition in an urban, coastal region in the US, Environ. Res. Commun., 2, 081001, 2020.

Kawashima, H. and Ono, S.: Nitrogen Isotope Fractionation from Ammonia Gas to Ammonium in Particulate Ammonium Chloride, Environ. Sci. Technol., 53, 10629–10635, 2019.

Kawashima, H., Ogata, R., and Gunji, T.: Laboratory-based validation of a passive sampler for determination of the nitrogen stable isotope ratio of ammonia gas, Atmospheric Environment, 245, 118009, 2021.

Kim, Y. P., Seinfeld, J. H., and Saxena, P.: Atmospheric gas-aerosol equilibrium I. Thermodynamic model, Aerosol Science and Technology, 19, 157–181, 1993.

Koutrakis, P., Wolfson, J. M., and Spengler, J. D.: An improved method for measuring aerosol strong acidity: results from a nine-month study in St Louis, Missouri and Kingston, Tennessee, Atmospheric Environment (1967), 22, 157–162, 1988.

Koutrakis, P., Sioutas, C., Ferguson, S. T., Wolfson, J. M., Mulik, J. D., and Burton, R. M.: Development and evaluation of a glass honeycomb denuder/filter pack system to collect atmospheric gases and particles, Environmental science & technology, 27, 2497–2501, 1993.

Li, M., Weschler, C. J., Beko, G., Wargocki, P., Lucic, G., and Williams, J.: Human ammonia emission rates under various indoor environmental conditions, Environmental Science & Technology, 54, 5419–5428, 2020.

Liu, J., Ding, P., Zong, Z., Li, J., Tian, C., Chen, W., Chang, M., Salazar, G., Shen, C., and Cheng, Z.: Evidence of rural and suburban sources of urban haze formation in China: a case study from the Pearl River Delta region, Journal of Geophysical Research: Atmospheres, 123, 4712–4726, 2018.

McIlvin, M. R. and Altabet, M. A.: Chemical Conversion of Nitrate and Nitrite to Nitrous Oxide for Nitrogen and Oxygen Isotopic Analysis in Freshwater and Seawater, Anal. Chem., 77, 5589–5595, https://doi.org/10.1021/ac050528s, 2005.

Meng, Z. Y., Lin, W. L., Jiang, X. M., Yan, P., Wang, Y., Zhang, Y. M., Jia, X. F., and Yu, X. L.: Characteristics of atmospheric ammonia over Beijing, China, Atmospheric Chemistry and Physics, 11, 6139–6151, 2011.

Muzio, L. J. and Arand, J. K.: Homogeneous Gas Phase Decomposition of Oxides of Nitrogen. Tustin, CA, KVB Incorporated, Electric Power Research Institute report FP-253, Project, 461, 1976.

Nowak, J. B., Huey, L. G., Russell, A. G., Tian, D., Neuman, J. A., Orsini, D., Sjostedt, S. J., Sullivan, A. P., Tanner, D. J., Weber, R. J., and others: Analysis of urban gas phase ammonia measurements from the 2002 Atlanta Aerosol Nucleation and Real-Time Characterization Experiment (ANARChE), Journal of Geophysical Research: Atmospheres (1984–2012), 111, 2006.

Pan, Y., Tian, S., Liu, D., Fang, Y., Zhu, X., Zhang, Q., Zheng, B., Michalski, G., and Wang, Y.: Fossil Fuel Combustion-Related Emissions Dominate Atmospheric Ammonia Sources during Severe Haze Episodes: Evidence from 15N-Stable Isotope in Size-Resolved Aerosol Ammonium, Environ. Sci. Technol., 50, 8049–8056, 2016.

Pan, Y., Tian, S., Liu, D., Fang, Y., Zhu, X., Gao, M., Gao, J., Michalski, G., and Wang, Y.: Isotopic evidence for enhanced fossil fuel sources of aerosol ammonium in the urban atmosphere, Environmental Pollution, 238, 942–947, 2018.

Pan, Y., Gu, M., Song, L., Tian, S., Wu, D., Walters, W. W., Yu, X., Lü, X., Ni, X., and Wang, Y.: Systematic low bias of passive samplers in characterizing nitrogen isotopic composition of atmospheric ammonia, Atmospheric Research, 105018, 2020.

Pandolfi, M., Amato, F., Reche, C., Alastuey, A., Otjes, R. P., Blom, M. J., and Querol, X.: Summer ammonia measurements in a densely populated Mediterranean city, Atmospheric Chemistry and Physics, 12, 7557–7575, 2012.

Park, R. J., Jacob, D. J., Field, B. D., Yantosca, R. M., and Chin, M.: Natural and transboundary pollution influences on sulfate-nitrate-ammonium aerosols in the United States: Implications for policy, Journal of Geophysical Research: Atmospheres, 109, 2004.

Parnell, A. C., Inger, R., Bearhop, S., and Jackson, A. L.: Source partitioning using stable isotopes: coping with too much variation, PloS one, 5, e9672, 2010.

Paulot, F., Jacob, D. J., Pinder, R. W., Bash, J. O., Travis, K., and Henze, D. K.: Ammonia emissions in the United States, European Union, and China derived by high-resolution inversion of ammonium wet deposition data: Interpretation with a new agricultural emissions inventory (MASAGE_NH_3), Journal of Geophysical Research: Atmospheres, 119, 4343–4364, 2014.

Paulot, F., Jacob, D. J., Johnson, M. T., Bell, T. G., Baker, A. R., Keene, W. C., Lima, I. D., Doney, S. C., and Stock, C. A.: Global oceanic emission of ammonia: Constraints from seawater and atmospheric observations, Global Biogeochemical Cycles, 29, 1165–1178, 2015.

Paulot, F., Ginoux, P., Cooke, W. F., Donner, L. J., Fan, S., Lin, M.-Y., Mao, J., Naik, V., and Horowitz, L. W.: Sensitivity of nitrate aerosols to ammonia emissions and to nitrate chemistry: implications for present and future nitrate optical depth, Atmospheric Chemistry and Physics, 16, 1459–1477, 2016.

Pekney, N. J., Davidson, C. I., Zhou, L., and Hopke, P. K.: Application of PSCF and CPF to PMF-modeled sources of $PM_{2.5}$ in Pittsburgh, Aerosol Science and Technology, 40, 952–961, 2006.

Perrino, C., De Santis, F., and Febo, A.: Uptake of nitrous acid and nitrogen oxides by nylon surfaces: Implications for nitric acid measurement, Atmospheric Environment (1967), 22, 1925–1930, 1988.

Plautz, J.: Piercing the haze, Science, 361, 1060–1063, 2018.

Puchalski, M. A., Rogers, C. M., Baumgardner, R., Mishoe, K. P., Price, G., Smith, M. J., Watkins, N., and Lehmann, C. M.: A statistical comparison of active and passive ammonia measurements collected at Clean Air Status and Trends Network (CASTNET) sites, Environmental Science: Processes & Impacts, 17, 358–369, 2015.

Reche, C., Viana, M., Pandolfi, M., Alastuey, A., Moreno, T., Amato, F., Ripoll, A., and Querol, X.: Urban NH_3 levels and sources in a Mediterranean environment, Atmospheric Environment, 57, 153–164, 2012.

Savard, M. M., Cole, A., Smirnoff, A., and Vet, R.: $\delta^{15}N$ values of atmospheric N species simultaneously collected using sector-based samplers distant from sources – Isotopic inheritance and fractionation, Atmospheric Environment, 162, 11–22, 2017.

Shah, V., Jaeglé, L., Thornton, J. A., Lopez-Hilfiker, F. D., Lee, B. H., Schroder, J. C., Campuzano-Jost, P., Jimenez, J. L., Guo, H., Sullivan, A. P., Weber, R. J., Green, J. R., Fiddler, M. N., Bililign, S., Campos, T. L., Stell, M., Weinheimer, A. J., Montzka, D. D., and Brown, S. S.: Chemical feedbacks weaken the wintertime response of particulate sulfate and nitrate to emissions reductions over the eastern United States, PNAS, 115, 8110–8115, 2018.

Song, L., Walters, W. W., Pan, Y., Li, Z., Gu, M., Duan, Y., Lü, X., and Fang, Y.: 15N natural abundance of vehicular exhaust ammonia, quantified by active sampling techniques, Atmospheric Environment, 255, 118430, 2021.

Stein, A. F., Draxler, R. R., Rolph, G. D., Stunder, B. J., Cohen, M. D., and Ngan, F.: NOAA's HYSPLIT atmospheric transport and dispersion modeling system, Bulletin of the American Meteorological Society, 96, 2059–2077, 2015.

Suarez-Bertoa, R., Zardini, A. A., and Astorga, C.: Ammonia exhaust emissions from spark ignition vehicles over the New European Driving Cycle, Atmospheric Environment, 97, 43–53, 2014.

Suarez-Bertoa, R., Mendoza-Villafuerte, P., Riccobono, F., Vojtisek, M., Pechout, M., Perujo, A., and Astorga, C.: On-road measurement of NH3 emissions from gasoline and diesel passenger cars during real world driving conditions, Atmospheric Environment, 166, 488–497, 2017.

Sun, K., Tao, L., Miller, D. J., Khan, M. A., and Zondlo, M. A.: On-Road Ammonia Emissions Characterized by Mobile, Open-Path Measurements, Environ. Sci. Technol., 48, 3943–3950, 2014.

Sun, K., Tao, L., Miller, D. J., Pan, D., Golston, L. M., Zondlo, M. A., Griffin, R. J., Wallace, H. W., Leong, Y. J., Yang, M. M., Zhang, Y., Mauzerall, D. L., and Zhu, T.: Vehicle Emissions as an Important Urban Ammonia Source in the United States and China, Environ. Sci. Technol., 51, 2472–2481, 2017.

Sutton, M. A., Dragosits, U., Tang, Y. S., and Fowler, D.: Ammonia emissions from non-agricultural sources in the UK, Atmospheric Environment, 34, 855–869, 2000.

Tomlin, A. S., Smalley, R. J., Tate, J. E., Barlow, J. F., Belcher, S. E., Arnold, S. J., Dobre, A., and Robins, A.: A field study of factors influencing the concentrations of a traffic-related pollutant in the vicinity of a complex urban junction, Atmospheric Environment, 43, 5027–5037, 2009.

Updyke, K. M., Nguyen, T. B., and Nizkorodov, S. A.: Formation of brown carbon via reactions of ammonia with secondary organic aerosols from biogenic and anthropogenic precursors, Atmospheric environment, 63, 22–31, 2012.

Urey, H. C.: The thermodynamic properties of isotopic substances, J. chem. Soc., 7, 562–581, 1947.

Uria-Tellaetxe, I. and Carslaw, D. C.: Conditional bivariate probability function for source identification, Environmental modelling & software, 59, 1–9, 2014.

Van Damme, M., Clarisse, L., Whitburn, S., Hadji-Lazaro, J., Hurtmans, D., Clerbaux, C., and Coheur, P.-F.: Industrial and agricultural ammonia point sources exposed, Nature, 564, 99, 2018.

Walker, J. T., Whitall, D. R., Robarge, W., and Paerl, H. W.: Ambient ammonia and ammonium aerosol across a region of variable ammonia emission density, Atmospheric Environment, 38, 1235–1246, 2004.

Walters, W. W. and Hastings, M. G.: Collection of Ammonia for High Time-Resolved Nitrogen Isotopic Characterization Utilizing an Acid-Coated Honeycomb Denuder, Anal. Chem., 90, 8051–8057, 2018.

Walters, W. W., Chai, J., and Hastings, M. G.: Theoretical Phase Resolved Ammonia–Ammonium Nitrogen Equilibrium Isotope Exchange Fractionations: Applications for Tracking Atmospheric Ammonia Gas-to-Particle Conversion, ACS Earth Space Chem., 2018.

Walters, W. W., Blum, D. E., and Hastings, M. G.: Selective Collection of Particulate Ammonium for Nitrogen Isotopic Characterization Using a Denuder–Filter Pack Sampling Device, Anal. Chem., 2019.

Walters, W. W., Song, L., Chai, J., Fang, Y., Colombi, N., and Hastings, M. G.: Characterizing the spatiotemporal nitrogen stable isotopic composition of ammonia in vehicle plumes, Atmospheric Chemistry and Physics, 20, 11551–11567, 2020.

Wang, S., Nan, J., Shi, C., Fu, Q., Gao, S., Wang, D., Cui, H., Saiz-Lopez, A., and Zhou, B.: Atmospheric ammonia and its impacts on regional air quality over the megacity of Shanghai, China, Scientific reports, 5, 15842, 2015.

Wu, L., Ren, H., Wang, P., Chen, J., Fang, Y., Hu, W., Ren, L., Deng, J., Song, Y., and Li, J.: Aerosol ammonium in the urban boundary layer in Beijing: insights from nitrogen isotope ratios and simulations in summer 2015, Environmental Science & Technology Letters, 6, 389–395, 2019.

Xiao, H.-W., Wu, J.-F., Luo, L., Liu, C., Xie, Y.-J., and Xiao, H.-Y.: Enhanced biomass burning as a source of aerosol ammonium over cities in central China in autumn, Environmental Pollution, 266, 115278, 2020.

Yao, X. and Zhang, L.: Trends in atmospheric ammonia at urban, rural, and remote sites across North America, Atmospheric Chemistry and Physics, 16, 11465–11475, 2016.

Yao, X., Hu, Q., Zhang, L., Evans, G. J., Godri, K. J., and Ng, A. C.: Is vehicular emission a significant contributor to ammonia in the urban atmosphere?, Atmospheric Environment, 80, 499–506, 2013.

Yu, X.-Y., Lee, T., Ayres, B., Kreidenweis, S. M., Jr, J. L. C., and Malm, W.: Particulate Nitrate Measurement Using Nylon Filters, Journal of the Air & Waste Management Association, 55, 1100–1110, 2005.

Yu, X.-Y., Lee, T., Ayres, B., Kreidenweis, S. M., Malm, W., and Collett, J. L.: Loss of fine particle ammonium from denuded nylon filters, Atmospheric Environment, 40, 4797–4807, 2006.

Zhang, L., Altabet, M. A., Wu, T., and Hadas, O.: Sensitive measurement of NH_4^+ $^{15}N/^{14}N$ ($\delta^{15}NH_4^+$) at natural abundance levels in fresh and saltwaters, Analytical chemistry, 79, 5297–5303, 2007.

Zhang, Y., Liu, X., Fang, Y., Liu, D., Tang, A., and Collett, J. L.: Atmospheric Ammonia in Beijing during the COVID-19 Outbreak: Concentrations, Sources, and Implications, Environ. Sci. Technol. Lett., 8, 32–38, 2021.

Zhou, C., Zhou, H., Holsen, T. M., Hopke, P. K., Edgerton, E. S., and Schwab, J. J.: Ambient Ammonia Concentrations Across New York State, Journal of Geophysical Research: Atmospheres, 124, 8287–8302, 2019.

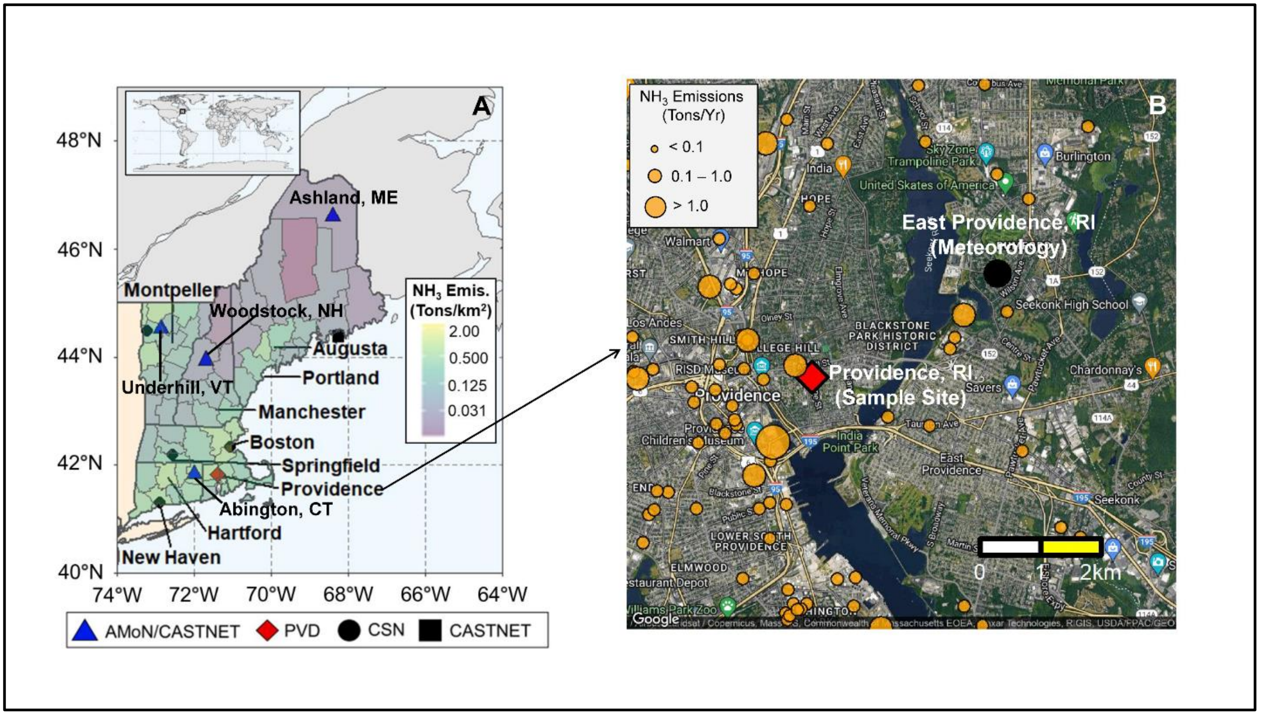

Figure 1. Overview of the sampling location in Providence, RI, USA (red diamond) located within New England (A) with the Ammonia Monitoring Network (AMoN)/Clean Air Status and Trends Network (CASTNET; blue triangle), Chemical Speciation Network (CSN; black circle), CASTNET only (black square) monitoring locations indicated. The counties in A are color-coded for NEI-14 NH_3 emission densities. The zoomed-in map of Providence, RI, US is shown in B with the sample site location (red diamond), the nearby CSN location with reported meteorology data (black circle) in East Providence, RI, USA, and the NH_3 point emission sources from the NEI (orange circles; size-coded to annual NH_3 emission) indicated. Image (B) was created using Google Maps (Map data ©2019 Google).

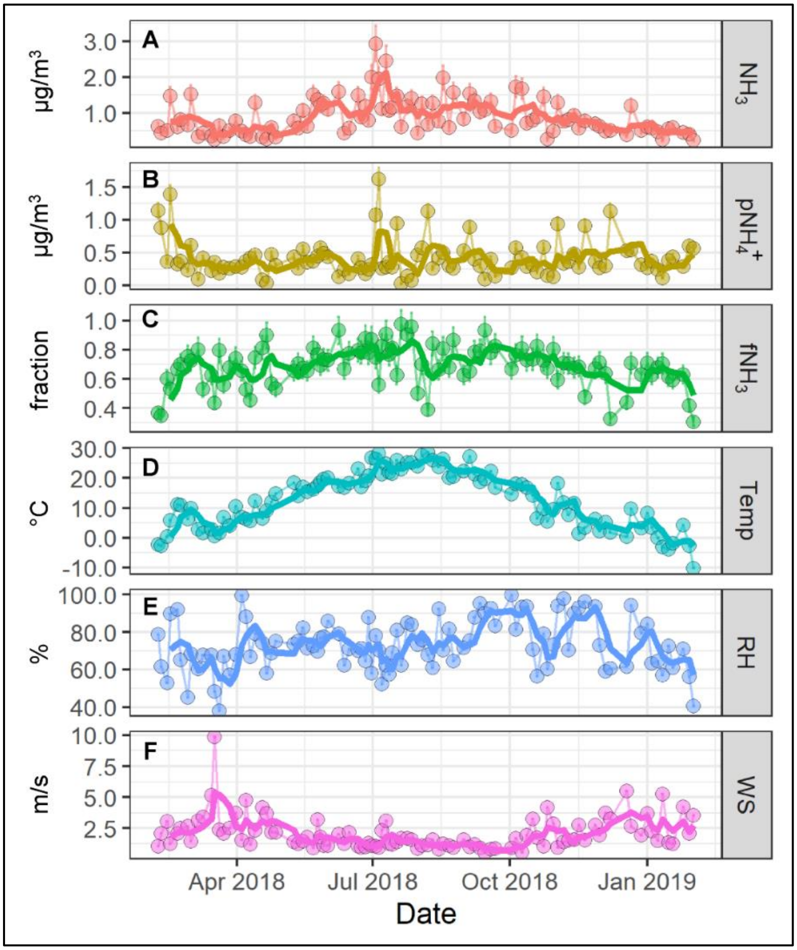

Figure 2. Time series plots of the measured NH_x data including (A) [NH_3], (B) [pNH_4^+], and (C) fNH_3 and the reported meteorology data including (C) temperature (Temp), relative humidity (RH), and wind speed (WS) from Feb 2018 – Feb 2019 in Providence, RI, US. The light data points refer to the 24-h integrated samples (A, B, C) or 24-h averaged meteorology data (D, E, F), and the dark lines represent approximate 2-week moving averages.

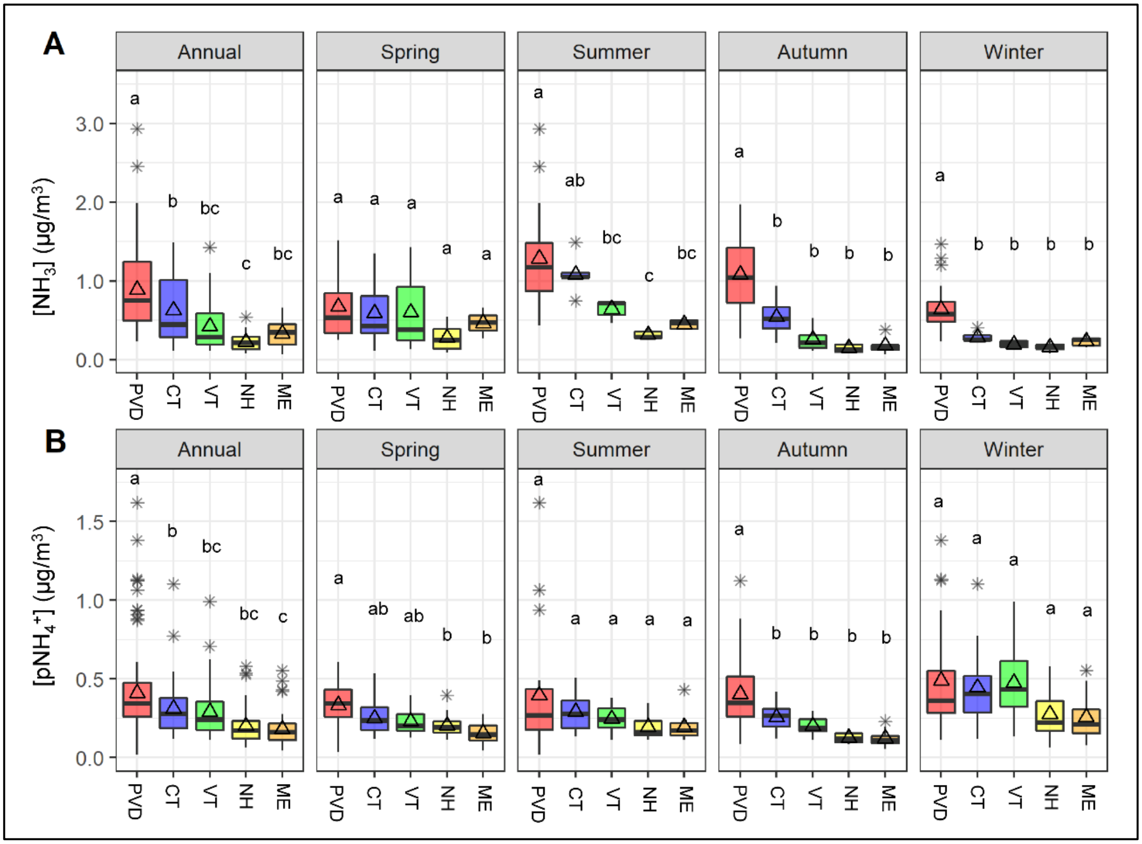

Figure 3. Box and whiskers plots that summarize the annual and seasonal (A) [NH_3] and (B) [pNH_4^+] distributions (lower extreme, lower quartile, median, upper quartile, and upper extreme) with the mean (open triangle) and outlier (black asterisk) at the Providence, RI (PVD) site and the New England AMoN/CASTNET sites including Abington, CT (CT), Underhill, VT (VT), Woodstock, NH (NH), and Ashland, ME (ME). Similar lowercase letters in the box and whiskers plots represent categories with statistically similar values.

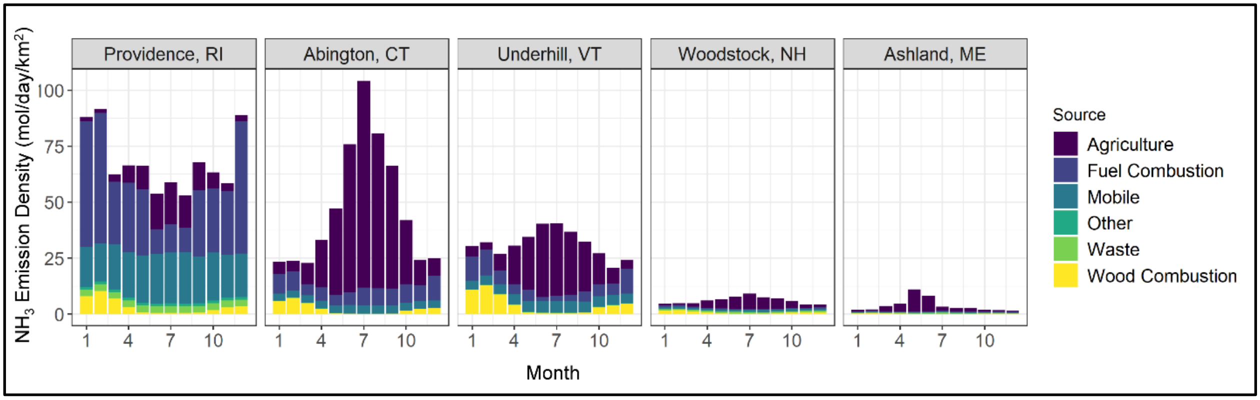

Figure 4. Monthly-based NH_3 emission densities speciated between agricultural, fuel combustion, mobile, other, waste, and wood combustion computed by the SMOKE model for the counties of the New England NH_3 monitoring site.

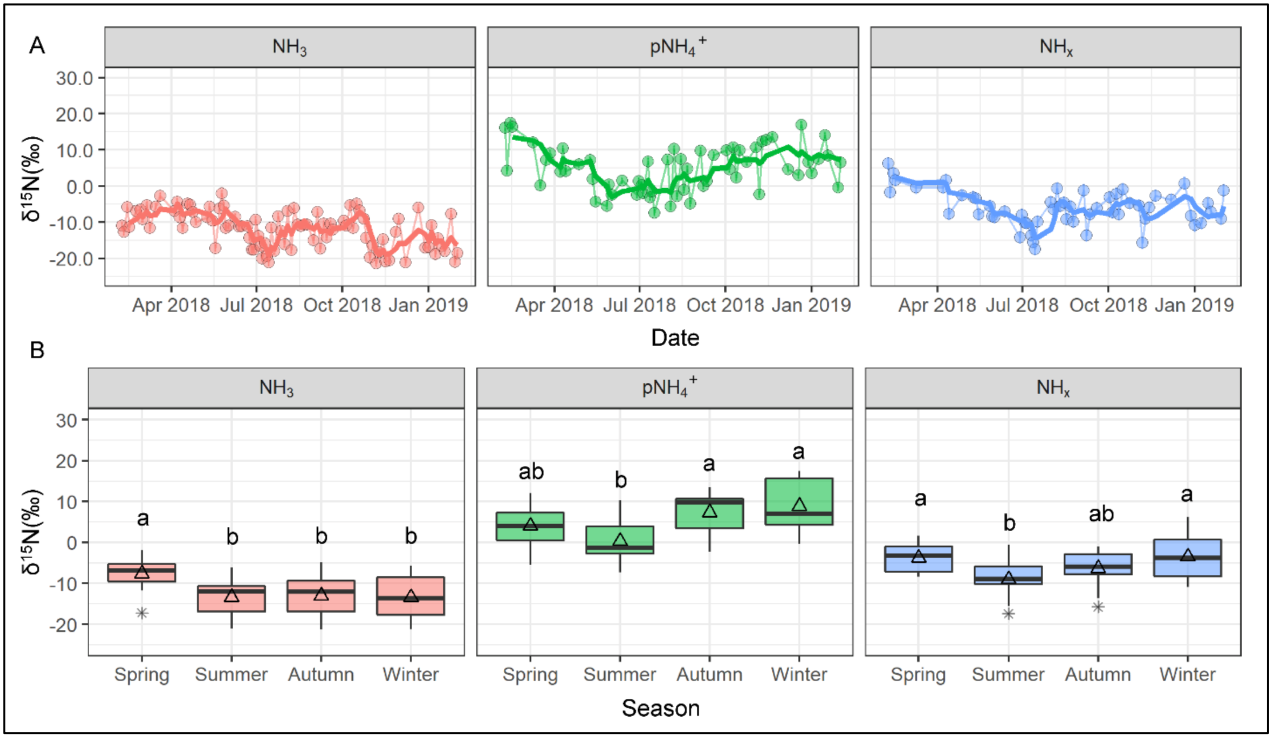

Figure 5. Measured δ^{15}N data of NH_3, pNH_4^+, and NH_x collected in Providence, RI, including (A) time series and (B) seasonal box and whiskers plots summarizing the distributions (lower extreme, lower quartile, median, upper quartile, and upper extreme) with the mean (open triangle) and outlier (black asterisk). Similar lowercase letters in the box and whiskers plots represent categories with statistically similar values.

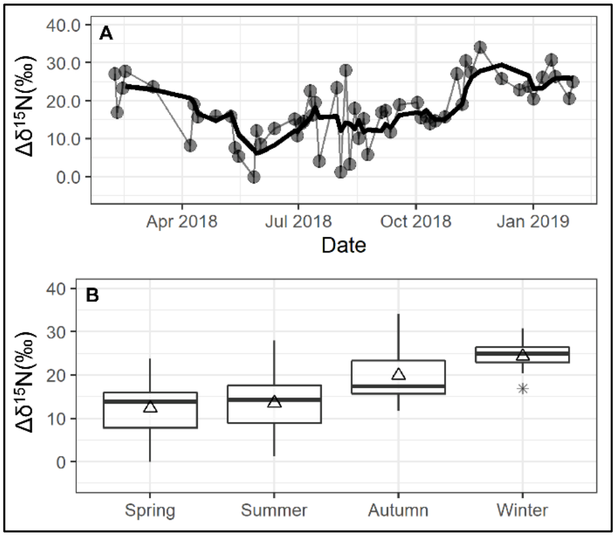

Figure 6. Seasonal $\Delta\delta^{15}N$ data at the Providence, RI monitoring site. In (A), the light data points and lines represent the observations, and the thick lines are four-point (~2 weeks) moving averages. (B) shows a box and whiskers plot summarizing the seasonal distributions (lower extreme, lower quartile, median, upper quartile, and upper extreme) with the mean (open triangle) and outlier (black asterisk).

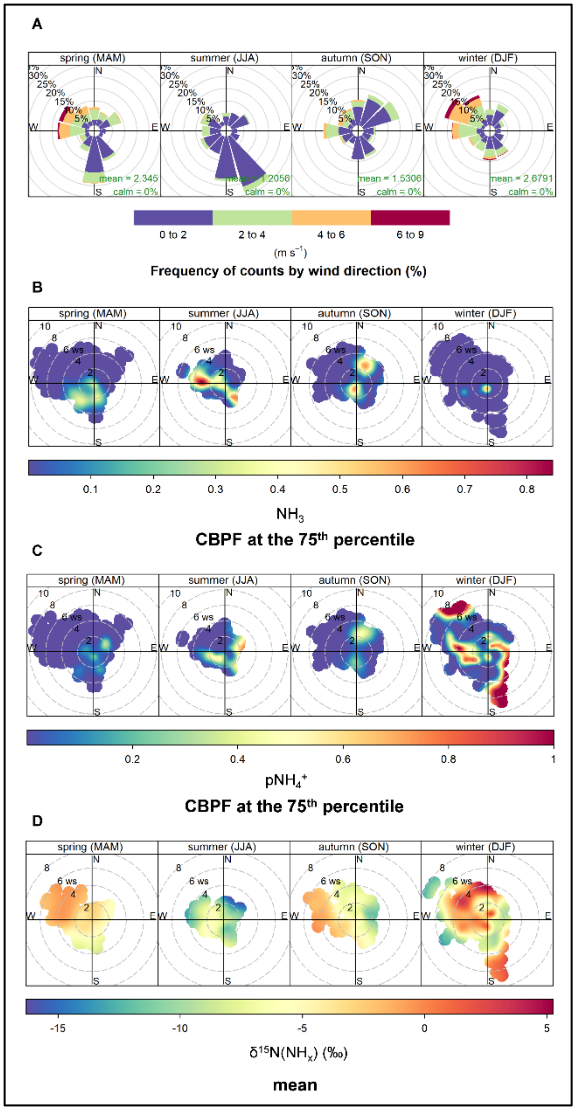

Figure 7. Overview of (A) windrose plots and polar bivariate (wind direction and wind speed) plots of the conditional bivariate probability function (CBPF) for (B) [NH_3] and (C) [pNH_4^+], and (D) mean $\delta^{15}N(NH_x)$ in Providence, RI, sorted by season.

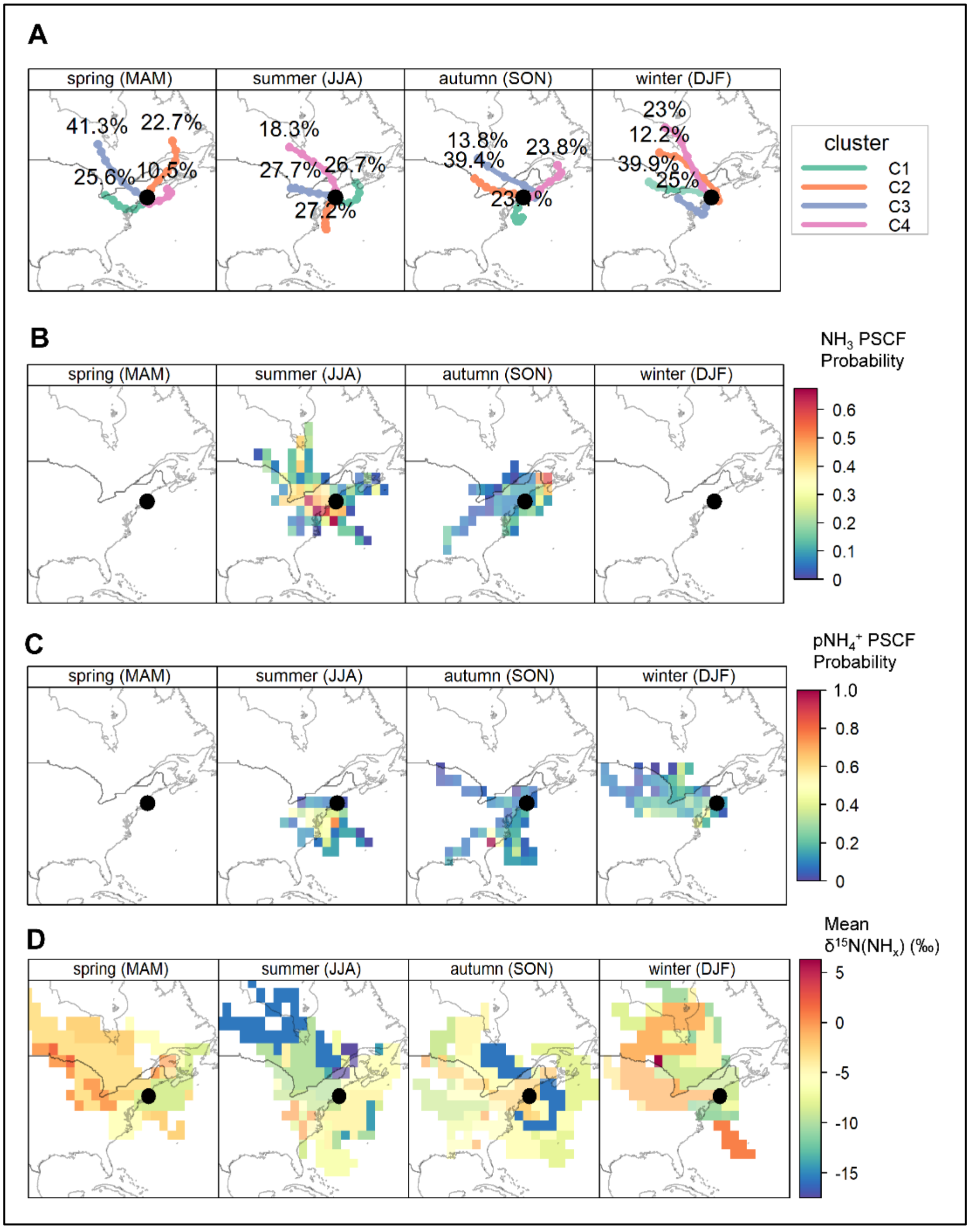

Figure 8. Influence of long-range transport including (A) clustered seasonal air mass back trajectories, (B) seasonal [NH_3] potential source contribution function probability (PSCF), (C) seasonal [NH_3] PSCF probability, and (D) seasonal air mass back trajectory
800 **$\delta^{15}N(NH_x)$ mean values.**

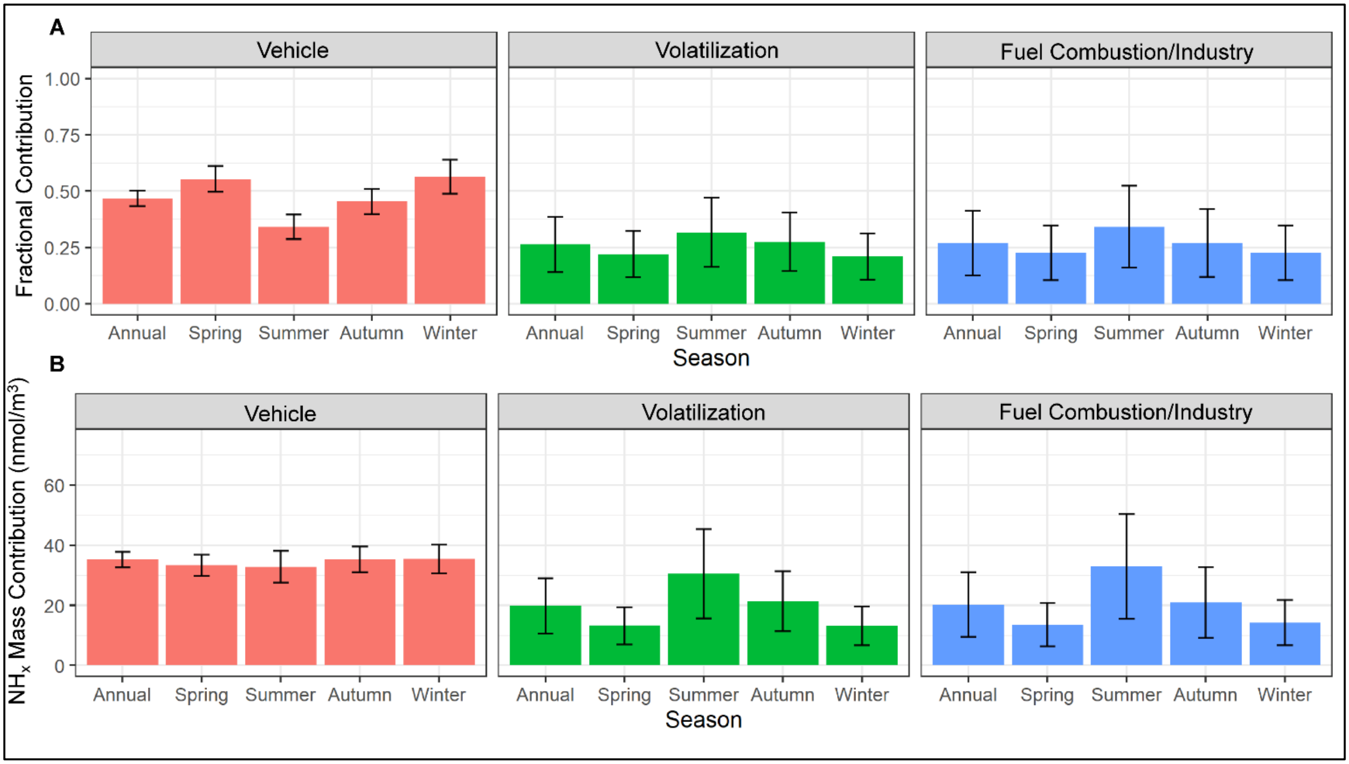

805

Figure 9. The calculated mean (A) fractional contribution and (B) mass weighted contributed of the major identified emission sources (Vehicle, Volatilization, Fuel Combustion/Industry) to NH_x in Providence, RI, utilizing a stable isotope mixing model (SIMMR). The error bars represent the standard deviation of the model simulations.